Morphology transitions induced by chemotherapy in carcinomas *in situ*

S. C. Ferreira, Jr.*
Departamento de Física, Instituto de Ciências Exatas, Universidade Federal de Minas Gerais, Caixa Postal 702, 30161-970 Belo Horizonte, Minas Gerais, Brazil

M. L. Martins†
Departamento de Física, Universidade Federal de Viçosa, 36571-000 Viçosa, Minas Gerais, Brazil

M. J. Vilela‡
Departamento de Biologia Animal, Universidade Federal de Viçosa, 36571-000 Viçosa, Minas Gerais, Brazil
(Received 20 December 2002; published 19 May 2003)

Recently, we have proposed a nutrient-limited model for the avascular growth of tumors including cell proliferation, motility, and death [S. C. Ferreira, Jr., M. L. Martins, and M. J. Vilela, Phys. Rev. E **65**, 021907 (2002)], which qualitatively reproduces commonly observed morphologies for carcinomas *in situ*. In the present work, we analyze the effects of distinct chemotherapeutic strategies on the patterns, scaling, and growth laws obtained for the nutrient-limited model. Two kinds of chemotherapeutic strategies were considered, namely, those that kill cancer cells and those that block cell mitosis but allow the cell to survive for some time. Depending on the chemotherapeutic schedule used, the tumors are completely eliminated, reach a stationary size, or grow following power laws. The model suggests that the scaling properties of the tumors are not affected by the mild cytotoxic treatments, although a reduction in growth rates and an increase in invasiveness are observed. For the strategies based on antimitotic drugs, a morphological transition in which compact tumors become more fractal under aggressive treatments was seen.

DOI: 10.1103/PhysRevE.67.051914 PACS number(s): 87.18.Hf, 87.18.Bb, 87.15.Vv

I. INTRODUCTION

Cancer is the uncontrolled cellular growth in which neoplastic cells invade adjacent normal tissues and give rise to secondary tumors (metastasis) on tissues or organs distant from its primary origin [1]. A cancer that remains confined within a messed surface, without break of the underlying basement membrane, is referred to as carcinoma *in situ*. *In situ* carcinoma is characterized by intense cytological atypia, necrosis, and frequent and abnormal mitosis, the tumor cells being arranged in various distinctive patterns [2]. A malignant tumor is derived from a single cell that, years before the tumor becomes clinically detectable, began an inappropriate pathway of proliferation [3]. Although cancers are extremely diverse and heterogeneous, a small number of pivotal steps associated to both deregulated cell proliferation and suppressed cell death are required for the development of any and all tumors. Indeed, all neoplasms evolve according to a universal scheme [4,5]. In the struggle against cancer, surgical removal, chemotherapy, and/or radiotherapy are the most commonly used treatments for the complete eradication of the tumor mass. Nowadays, new approaches, such as immunotoxins [6], gene [7], antiangiogenic [8], and virus [9] therapies, are being developed and have been successfully used in the treatment of several kinds of experimental and human tumors.

Mathematical models are always used as a tentative for describing cancer growth. In particular, numerous models based on classical reaction-diffusion equations have been proposed to investigate the growth of tumor spheroids [10], cancer progress and its interaction with the immune system [11], and the tumor angiogenesis [12,13]. Fractal growth patterns in gliomas (brain tumors) were recently investigated by Sander and Deisboeck [14]. Recently, we have studied a diffusion-limited model for the growth of carcinomas *in situ*, in which cell proliferation, motility, and death are locally controlled by growth factors [15,16]. This model generates compact, connected, and disconnected morphologies characterized by the Gompertzian growth in time and distinct scaling laws for the tumor interfaces. These patterns result from a competition between cancer cell division and migration, both directed outwards the growth factor concentration gradient, and cell death. Depending on the parameters controlling the cell response to the degradation rate of growth factors, morphology transitions from disconnected to compact patterns and from disconnected to connected patterns are observed. In order to generate papillary and ramified morphologies found in many epithelial cancers and trichoblastomas, we were led to analyze the effects of nutrient competition in cancer development [17].

In addition to the vast literature dedicated to tumor growth modeling, many research papers addressing cancer therapies have recently been published. Indeed, cancer cell kinetics under treatments using antimitotic agents [18,19], radiotherapy [20,21], virus that replicates selectively in tumor cells [22], antiangiogenic chemicals [23], as wells as the effects of tumor drug resistance and tumor vasculature on chemotherapies [24] were studied using mathematical models. It is worthwhile to mention that the literature related to

*Electronic address: silviojr@fisica.ufmg.br
†Electronic address: mmartins@ufv.br
‡Electronic address: marcelo@ufv.br

 ©2003 The American Physical Society

cancer growth and therapy is enormous, and there is much activity by mathematicians, physicists, and theoretical biologists. Thus, the above cited references constitute a partial selection chosen according to the authors' research interest.

In this paper, we analyze the effects of distinct chemotherapeutic strategies in the model for the growth of avascular tumors proposed by us [17]. Specifically, we are interested in possible changes in the tumor patterns, scaling, and growth laws reported in the original model triggered by chemotherapies. The paper is organized as follows. In Sec. II the nutrient-limited model for cancer growth and its main results are reviewed. In Sec. III, chemotherapeutic treatments that aim to kill cancer cells are introduced in the framework of the present model and their effects discussed. In Sec. IV, a model for chemotherapy with antimitotic agents is considered. Finally, we draw some conclusions in Sec. V.

II. THE NUTRIENT-LIMITED MODEL

Our nutrient-limited model combines macroscopic reaction-diffusion equations, describing the nutrient field concentration, with microscopic stochastic rules governing the actions of individual tumor cells. The basic principles included in the model are cell proliferation, motility, death, as well as competition for nutrients among cancer and normal cells. Also, the nutrient concentration field locally controls cell division, migration, and death.

A. The model

1. The tissue

The tissue, represented by a square lattice of size $(L+1)\times(L+1)$ and lattice constant Δ, is fed by a single capillary vessel at $x=0$, i.e., the top of the lattice. The capillary is the unique source from which nutrients diffuse through the tissue towards the individual cells. Although a tumor mass is composed of different cell subpopulations [4], the model considers only three types: normal, cancer, and tumor dead cells. Any site, with coordinates $\vec{x}=(i\Delta,j\Delta)$, $i,j=0,1,2,\ldots,L$, is occupied by only one of these cell types. In contrast to the normal cells, one or more cancer cells can pile up in a given site. In turn, dead tumor cells are inert. Thus, each lattice site can be thought of as a group of cells in which the normal, dead, and cancer cell populations assume one of the possible values $\sigma_n(\vec{x})=\sigma_d(\vec{x})=0,1$ and $\sigma_c(\vec{x})=0,1,2,\ldots$, respectively. According to the theory of the monoclonal origin of cancer [3], a single cancer cell at $y=L\Delta/2$ and at a distance X from the capillary is introduced in the normal tissue. Periodic boundary conditions along the horizontal axis are used. The row $i=0$ represents the capillary vessel and the sites with $i=L+1$ constitute the external border of the tissue. This geometry is particularly adequate to describe the growth of carcinomas (epithelial tumors) *in situ* because the present model considers that the tumor mass receives nutrients only by diffusion from the capillary vessel. However, the model can be extended to other cancers.

2. The nutrients

The nutrients are divided into two classes: essential to cell proliferation, those necessary for DNA synthesis, and nonessential to cell division. The essential and nonessential nutrients are described by the concentration fields $N(\vec{x},t)$ and $M(\vec{x},t)$, respectively. These nutrient fields obey the dimensionless diffusion equations (see Ref. [17] for the complete variable transformations)

$$\frac{\partial N}{\partial t}=\nabla^2 N-\alpha^2 N\sigma_n-\lambda_N\alpha^2 N\sigma_c \tag{1}$$

and

$$\frac{\partial M}{\partial t}=\nabla^2 M-\alpha^2 M\sigma_n-\lambda_M\alpha^2 M\sigma_c, \tag{2}$$

in which differentiated nutrient consumption rates for normal and cancer cells by factors λ_N and λ_M are assumed. It is important to notice that the model admits the simplest form for the nutrient diffusion, i.e., linear equations with constant coefficients. This assumption seems to be an acceptable first approach, since only the initial avascular stages of tumor growth, involving a relatively small number of cancer cells, are considered. So, nonlinear effects on the diffusion processes are expected to be minimal. Also, $\lambda_N>\lambda_M$ is used, reflecting the larger affinity of cancer cells for essential nutrients.

The boundary conditions satisfied by the normalized nutrient concentration fields are $N(x=0)=M(x=0)=1$, representing the continuous and fixed supply of nutrients provided by the capillary vessel. The hypothesis that a blood vessel provides a fixed nutrient supply to the cells in a tissue is a simplification that neglects the complex response of the vascular system to the metabolic changes of cell behavior [25]. $N(y=0)=N(y=L)$ and $M(y=0)=M(y=L)$, corresponding to the periodic boundary conditions along the y axis, used in order to minimize edge effects and, therefore, better simulate an extended tissue. At last, Neumann boundary conditions, $\partial N(x=L)/\partial x=\partial M(x=L)/\partial x=0$, are imposed to the border of the tissue, meaning that the nutrients cannot traverse the external layer of the epithelial tissue.

3. Cell dynamics

In our original model, each tumor cell, randomly selected with equal probability, can carry out one of the three actions: division, migration, or death. However, in the present work we consider just the accommodation that happens during cell mitosis among the daughter cells. Consequently, each tumor cell can carry out one of the following two actions.

(*a*) *Division*. Cancer cells divide by mitosis with probability P_{div}. If the chosen cell is inside the tumor, its daughter will pile up at that site, and $\sigma_c(\vec{x})\rightarrow\sigma_c(\vec{x})+1$. Otherwise, if the selected cell is on the tumor border, its daughter cell will occupy at random one of their nearest neighbor sites $\vec{x}'$ containing a normal or a necrotic cell and, therefore, $\sigma_c(\vec{x}')=1$ and $\sigma_{n,d}(\vec{x}')=0$. The mitotic probability P_{div} is deter-

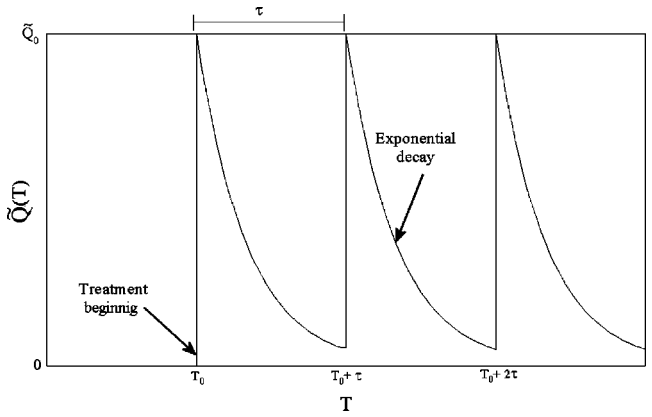

FIG. 1. Temporal profile of drug concentration at the capillary vessel.

mined by the concentration per cancer cell of the essential nutrients N present on the microenvironment of the selected cell:

$$P_{div}(\vec{x}) = 1 - \exp\left[-\left(\frac{N(\vec{x})}{\sigma_c(\vec{x})\,\theta_{div}} \right)^2 \right]. \tag{3}$$

The Gaussian term is included in order to produce a sigmoid curve saturated to unity, and the model parameter θ_{div} controls the shape of this sigmoid.

(*b*) *Death*. Cancer cells die with probability P_{del}. Thus, $\sigma_c(\vec{x}) \to \sigma_c(\vec{x}) - 1$ and $\sigma_d(\vec{x}) = 1$ when σ_c vanishes. The cell death probability P_{del} is determined by the concentration per cancer cell of the nonessential nutrients M present on the microenvironment of the selected cell:

$$P_{del}(\vec{x}) = \exp\left[-\left(\frac{M(\vec{x})}{\sigma_c(\vec{x})\,\theta_{del}} \right)^2 \right], \tag{4}$$

i.e., a Gaussian distribution whose variance depends on the model parameter θ_{del}.

The biological basis for these cell dynamic rules can be found in Ref. [17]. However, it is worthwhile to notice that from the point of view of the so-called kinetic cellular theory, which provides a general framework for the statistical description of the population dynamics of interacting cells [11], the local probabilities P_{div} and P_{del} can be thought of as an effective kinetic cellular model.

4. Computer implementation

The growth model simulations were implemented using the following procedure. At each time step T, Eqs. (1) and (2) are numerically solved in the stationary state ($\partial N/\partial t = \partial M/\partial t = 0$) through relaxation methods. Provided the nutrient concentration at any lattice site, $N_C(T)$ cancer cells are sequentially selected at random with equal probability. For each one of them, a tentative action (division or death) is randomly chosen with equal probability and the time is incremented by $\Delta T = 1/N_C(T)$. The selected cell action will be implemented or not according to the correspondent local probabilities determined by Eq. (3) or (4). At the end of this

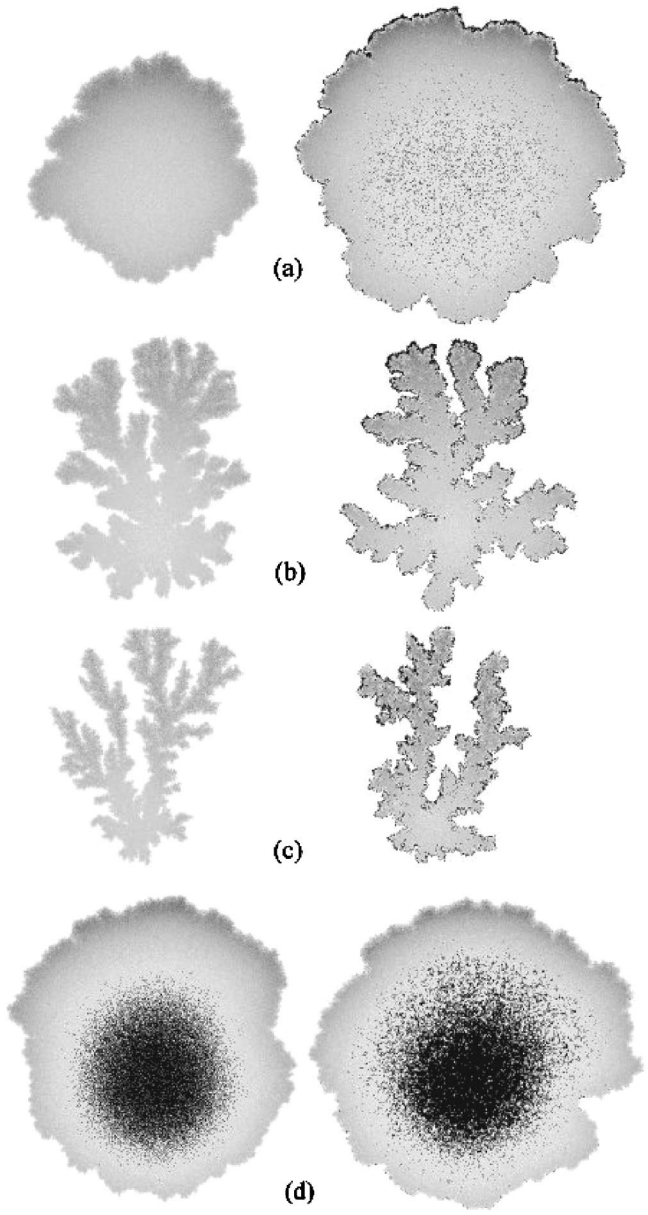

FIG. 2. Tumor growth patterns generated by the limited-nutrient model under chemotherapeutic treatment. The patterns are drawn on a gray scale; where the darker gray regions represent higher cancer cell populations, the black points represent the sites occupied by necrotic cells, and the white regions represent the normal tissue. The tissue size is 500×500, and the initial ''cancer seed'' is 300 sites distant from the capillary. The total number of cancer cells depends on tumor morphology and reach up to 2×10^5 for compact patterns. Two typical patterns, without (left) and with soft treatment (right) are shown for (a) compact, (b) papillary, (c) ramified morphologies, and (d) patterns with a necrotic core. The fixed parameters used to generate these morphologies are listed in Table I. Mild treatment means that the period between two doses is large ($\tau = 20$) and, therefore, the tumor grows continuously. The other parameters are $\theta_{del}^{(Q)} = 0.1$ and $N_0 = 10^4$.

sequence of $N_C(T)$ tentatives, a new time step begins and the entire procedure (solution of the diffusion equations and application of the cell dynamics) is iterated. The simulations stop if any tumor cell reaches the capillary vessel.

B. Main results

The model reproduces commonly observed tumor morphologies including the papillary, compact, and ramified patterns shown in Fig. 2. The nutrient consumption by normal and cancer cells, controlled by the model parameters α, λ_N, and λ_M, plays a central role in morphology selection. For small values of these parameters, corresponding to growth conditions in which individual cells demand small nutrient supplies, the patterns tend to be compact and circular [Fig. 2(a)]. However, if the mitotic rate of cancer cells is small due to the large amount of nutrients demanded for cell division, generating a significant competition for nutrients, these compact patterns progressively assume papillarylike morphologies [Fig. 2(b)]. At high nutrient consumption rates these papillary patterns become the rule and, for low cancer cell division, continuously transform into thin tips, filaments, or chords of cells (Fig. 2c). Also, the model generates patterns with an inner core of died cells for high nutrient consumption or cell division rates [Fig. 2(d)]. As observed in *in vivo* tumors and *in vitro* multicell spheroids [10], these simulated patterns consist of three distinct regions: a central necrotic core, an inner rim of quiescent cancer cells, and a narrow outer shell of proliferating cells.

The tumor patterns generated by our nutrient-limited model were characterized by its gyration radius R_g, total number of cancer cells N_C, and number of sites on tumor periphery S (including the surface of holes, if any). The gyration radius R_g is defined as

$$R_g = \left(\frac{1}{n} \sum_{i=1}^{n} r_i^2 \right)^{1/2}, \tag{5}$$

where n is the number of sites occupied by the pattern (cancer or necrotic cells) and r_i is the distance of the occupied site i from the tumor mass center. These quantities could be related to clinically important criteria such as progress curves, growth rates (volumetric doubling time) at given radii, and proliferative and necrotic fractions of the tumor.

The progress in time of cancer cell populations for all the simulated patterns follows the Gompertz curves:

$$N_C(T) = A \exp\{-\exp[-k(T-T_c)]\}, \tag{6}$$

representing an initial exponential growth that is saturated in larger times.

Alternatively, as a function of the number of sites occupied by the pattern, n, both R_g and S obey power law scalings given by $R_g \sim n^{\nu}$ and $S \sim n^{\sigma}$, respectively. For solid patterns these exponents are $\nu \sim 0.5$ and $\sigma \sim 0.5$, corresponding to effective circular and nonfractal patterns. As the nutrient consumption increases, the patterns tend to papillarylike shapes for which the exponent σ increases towards the value 1 and the exponent ν varies in the range [0.50,0.60], indicating a fractal morphology for the tumor.

III. CYTOTOXIC CHEMOTHERAPEUTIC DRUGS

The prime objective of the antitumoral treatment with chemotherapeutic drugs is to kill or at least to stop the proliferation of the cancer cells. In general, the drugs should act only on proliferating cells, mainly the cancer ones. However, drugs also destroy proliferating normal cells promoting several collateral effects [26]. Indeed, epithelial cells from the respiratory and gastrointestinal systems, which frequently reproduce in order to substitute their dead counterparts, are strongly affected. In this section, we analyze a simple chemotherapeutic model in which the complex details of the cell-cycling responses to the drugs are taken into account by an effective kinetic model.

A. The model

As used in previous works [27], the chemotherapy is modeled by a periodic delivery of cytotoxic drugs through the same capillary vessel supplying the nutrients to the tissue. Several cytotoxic drugs and their properties were exhaustively studied such as amsacrine, cisplatin, cyclophosphamide, cytarabine, mustine, and anthracycline [28]. Here, the numerous barriers involved in tumor drug delivery [29] were not considered, and the treatment begins when the tumor mass contains N_0 cancer cells. When a dose is applied, the drug concentration in the capillary assumes a maximum value $\tilde{Q}_0$, which progressively decreases due to the gradual drug elimination by the organism. Hence, new doses are periodically administered at time intervals τ in most of the chemotherapeutic strategies [28]. Various functional forms for time evolution of drug concentration have been considered in therapy models [27]. Here, we adopt a realistic model in which the drug concentration at the capillary, $\tilde{Q}(T)$, is a function of time written as

$$\tilde{Q}(T) = \begin{cases} 0 & \text{if } T < T_0 \\ \tilde{Q}_0 \exp[-(T - l\tau)/T_\times] & \text{if } T_0 + l\tau \leqslant T < T_0 + (l+1)\tau, \end{cases} \tag{7}$$

where $l = 0,1,2,\ldots$ is the number of applied doses, T_x is the characteristic time for the drug elimination by the organism, and T_0 is the time at which the treatment begins. The functional form of $\tilde{Q}(T)$ is shown in Fig. 1.

As the nutrients, drugs also diffuse from the capillary vessel toward the individual cells, and their concentration $Q(\vec{x},t)$ at any lattice site at each time step is given by the stationary solution of the diffusion equation

$$\frac{\partial Q}{\partial t} = D_Q \nabla^2 Q - \Gamma^2 Q - \lambda_Q \Gamma^2 Q \sigma_c . \tag{8}$$

The first, second, and third terms on the right hand side represent drug diffusion, natural degradation, and absorption by cancer cells, respectively. Again, this equation is the simplest one describing the diffusion phenomenon. Equation (8) is written using the same dimensionless variables of Eqs. (1)

TABLE I. Fixed parameters used in tumor growth simulations under chemotherapeutic treatment for each morphology type.

Morphology	λ_N	λ_M	λ_Q	α	Γ	θ_{div}	θ_{del}	T_x
Compact	25	10	10	$2/L$	$2/L$	0.3	0.03	4
Papillary	200	10	10	$2/L$	$2/L$	0.3	0.03	4
Ramified	200	10	10	$3/L$	$2/L$	0.3	0.01	4
Necrotic	50	25	10	$3/L$	$2/L$	0.3	0.03	4

and (2). Also, the parameters $\tilde{Q}_0$ and D_Q can be made equal to unity without loss of generality. The boundary conditions are the same as those used for the nutrient fields, except at the capillary vessel where the concentration at each time step is given by Eq. (7).

Finally, a single change is introduced into the cell dynamics described in Sec. II: an additional chance of death occurs whenever a cancer cell enters mitosis. Thus, every time a cancer cell divides, each one of the generated cells can die with probability

$$P_{del}^{(Q)}(\vec{x}) = 1 - \exp\left[-\left(\frac{Q(\vec{x})}{\sigma_c(\vec{x})\,\theta_{del}^{(Q)}} \right)^2 \right]. \qquad (9)$$

The parameter $\theta_{del}^{(Q)}$ controls the cell sensitivity to the drugs. Also, because in the original nutrient-limited model the normal cells do not take part in the cell dynamics, i.e., they do not divide or die, we disregard the chemotherapeutic effects on normal cells.

B. Results

The main aim of this work was to investigate the effects of treatments on the various morphologies, and scaling and growth laws observed in the original model. Thus, for each morphology, determined by the fixed parameters reported in Table I, the treatment parameters, namely, τ (the dose period), $\theta_{del}^{(Q)}$ (drug efficiency), and N_0 (tumor size at the treatment beginning) were varied. Such parameters can be directly tested in the laboratory. The remaining parameters (λ_Q, Γ, and $T_\times$) associated with drug diffusion and elimination were also fixed in all the simulations.

In Fig. 2, the corresponding patterns for compact, papillary, and ramified morphologies with and without treatment are shown. In this figure the treatment is not able to cease tumor development. As can be seen, the morphological tumor patterns do not change under mild treatment. However, the regions occupied by the tumors are larger than those without treatment. These results suggest that the direct attack to the tumor might be an inadequate treatment strategy. Indeed, the more invasive is the tumor, the higher is the possibility of the cancer cells to reach the capillary vessel and, consequently, metastasize successfully. Such result is in agreement with Israel's claim [30] that cancer cells trigger adaptation mechanisms in stress circumstances similar to those observed in bacterial colonies. Moreover, in our model neither genetic nor epigenetic changes are necessary to explain the increase of tumor aggressiveness. It naturally emerges from the growth rules. A tumor submitted to successive chemotherapeutic treatments that do not lead to its complete eradication may progressively become more resistant, aggressive, and malignant.

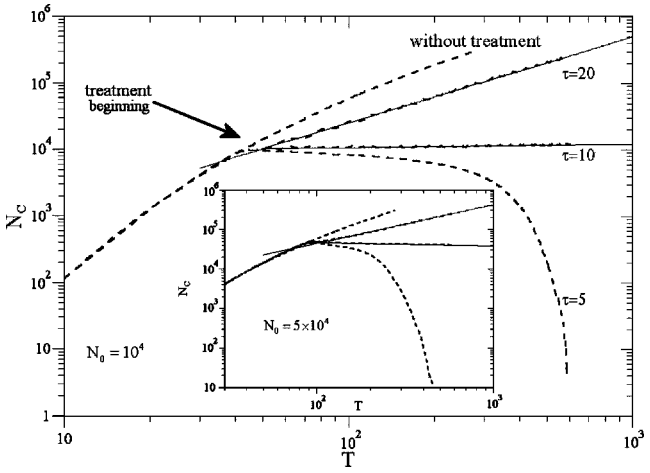

FIG. 3. Growth curves for compact patterns (dashed lines). Three dose intervals were tested ($\tau=5,10,20$) in tumors with two distinct initial sizes: $N_0=10^4$ and $N_0=5\times10^4$ (inset). The exponents of the power laws (slopes of the straight lines) are 1.3 (0.98) for the tumors with $N_0=10^4$ ($N_0=5\times10^4$) when $\tau=20$, and 0.05 (-0.09) when $\tau=10$. Times are in arbitrary units.

Very similar scaling laws $R_g \sim n^\nu$ and $S \sim n^\sigma$ for the treated tumors were observed (ν and σ values are reported in Ref. [17]). The small differences in the exponent values for the number of tumor peripheral sites vanishes at the asymptotical limit of tumor size. This exponent invariance suggests that the fractal morphology is a robust aspect of these tumors and cannot be changed by small perturbations in the cell microenvironment. Obviously, the scaling laws for R_g and S are not defined for the tumors that cease their growth.

We have also studied the influence of the treatment parameters (τ, $\theta_{del}^{(Q)}$, N_0) on the tumor growth curves. In Fig. 3, the evolution in time of the total number of cancer cells for compact tumors is shown. Depending on the dose period τ the tumors may disappear, saturate their growth, or progress according to power laws. Actually, the time interval between two consecutive doses is a fundamental clinical feature determining the treatment success. The power law regime observed when τ is large means a slow progress, neatly contrasting with the exponential growth present in the Gompertz law describing tumor progress without chemotherapy. The tumor size at the beginning of the treatment is another important factor. Indeed, the exponents of the power laws characterizing the tumor growth are smaller when the initial tumor size is larger. This scenario seems to be universal. Sometimes, as shown Fig. 3, compact tumors that began to receive drug doses at regular intervals of $\tau=5$ when it contained $N_0=10^4$ cancer cells were eliminated slower than another one that began to be treated with $N_0=5\times10^4$ cancer cells. However, this is not the rule. For example, simulations of papillary tumors indicate that smaller tumors are faster eliminated when $\tau=5$. Finally, since the growth law exponents depend on the parameter sets used, they are not uni-

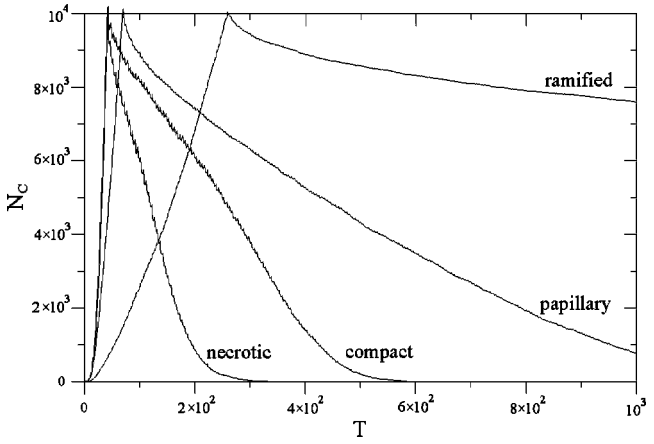

FIG. 4. Growth curves for distinct tumor morphologies. The doses were applied at intervals $\tau=5$ in tumors with initial sizes $N_0=10^4$. Times are in arbitrary units.

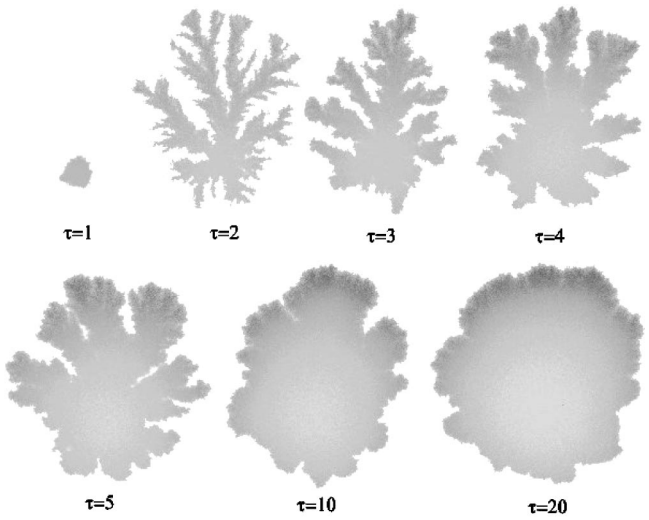

FIG. 5. Compact patterns under treatment with antimitotic drugs. The dose period τ was varied and $\theta_{div}^{(Q)}=0.3$ was fixed. The other parameters are indicated in Table I. Tumors become more and more fractal as the dose period decreases. At a critical period the tumors reach a frozen state in which their sizes remain constant during all the treatments.

versal. Concerning the $\theta_{del}^{(Q)}$ parameter, it just modifies the treatment efficiency.

Fractal tumors are more resistant to treatments. In Fig. 4, the growth curves $N_C \times T$ are drawn for compact, papillary, ramified, and necrotic morphologies shown in Fig. 2. One can see that the more fractal is the tumor larger is the required time to eliminate it. Indeed, the lower growth rates of fractal tumors imply on a large fraction of cancer cells maintained at a quiescent state. So, since chemotherapeutic drugs considered in this model only act in the dividing cells, the treatment becomes inefficient when the major fraction of the cancer cells are quiescent.

In addition, we have studied tumor patterns exhibiting a central necrotic core. The results for cancer growth and the correspondent power laws are similar to those found for compact patterns. The density of cancer cells and their average division rates through the growth patterns are not significatively altered when the tumors are submitted to mild treatments (long time intervals between consecutive drug doses). Moreover, their growth patterns are very similar to those found in the untreated counterparts. Finally, tumors exhibiting necrotic cores are more easily eliminated when shorter periods of the drug administration are considered (Fig. 4).

IV. ANTIMITOTIC CHEMOTHERAPEUTIC DRUGS

Several drugs used in cancer chemotherapies do not kill cancer cells. Instead, they aim to stop the cell cycle in specific checkpoints. As a consequence of that, the tumors cease or slow down their growth rate. Examples of such drugs include the antimitotic agent curacin *A* that blocks the cell cycle in the *M* phase, mitomycin *C*, doxorubicin, and aclarubicin, among others [28]. In order to analyze the effects of drugs that inhibit cell division on tumor patterns, we introduce a very simple change in the cell dynamics of the model described in the preceding section. Instead of an additional death probability given by Eq. (9), the division probability is modified by including an additional term in Eq. (3). So, the new division probability becomes

$$P_{div}=1-\exp\left[-\left(\frac{N}{\sigma_c\theta_{div}}\right)^2+\left(\frac{Q}{\sigma_c\theta_{div}^{(Q)}}\right)^2\right], \qquad (10)$$

in which the first and second terms in the exponential argument compete between themselves stimulating and inhibiting the cell mitosis, respectively. The parameter $\theta_{div}^{(Q)}$ controls the drug influence on the cell division. Obviously, if the exponential argument is positive, then $P_{div}\equiv 0$.

The biological interpretation of the present model is very distinct from that considered in the preceding section. Now, the drugs modify the intrinsic characteristics of the cancer cells and, consequently, the tumors must behave in a different manner from those treated with cytotoxic agents. Indeed, as one can see in Fig. 5, a morphological transition for the tumor patterns when the dose periods decrease is observed. If the period is sufficiently short, the tumor size remains constant during the therapy. Obviously, the critical period depends on other model parameters, especially on $\theta_{div}^{(Q)}$. In order to see this dependence, the critical value of $\theta_{div}^{(Q)*}$ for which the tumors cease their growth with probability 1 as a function of τ was evaluated. A mean field analysis of Eq. (10) provides $\theta_{div}^{(Q)} \sim \exp(-\tau/T_x)$, in agreement with the simulations as indicated in Fig. 6. Thus, an exponential decay with a universal characteristic length T_x was found, which is independent of the other model parameters. This law, relating two important clinical parameters, is valid for a wide set of parameter values. In addition to the compact tumors shown in Fig. 5, papillary tumors were also simulated under antimitotic treatment, and a similar morphology transition was observed.

Figure 7 shows that these morphological transitions occurred at well defined $\theta_{div}^{(Q)}$ values. Near the critical value, instabilities in the reaction-diffusion equations lead to a

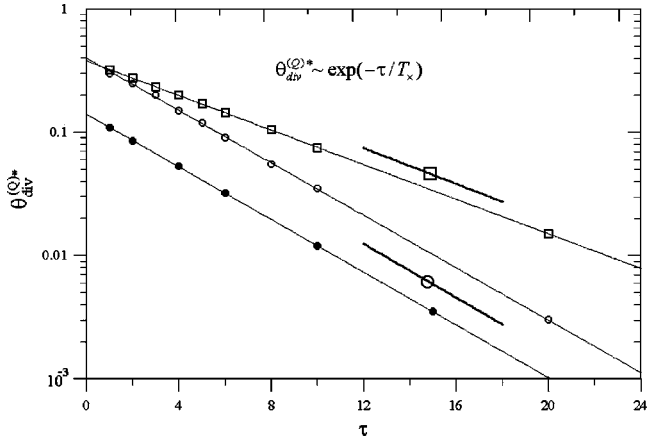

FIG. 6. Critical values $\theta_{div}^{(Q)*}$ as a function of the dose period τ. The symbols represent simulational data and the straight lines the respective exponential fittings. The open circles refer to the simulations using the parameters for the compact patterns listed in Table I. The squares (filled circles) represent the same simulations, except that $T_\times = 6$ ($\theta_{div} = 0.1$). Also, the slopes 1/4 (circle) and 1/6 (square) are indicated. In order to estimate $\theta_{div}^{(Q)*}$, we realized 20 independent simulations for each value of $\theta_{div}^{(Q)}$ and considered that the growth failure for all these tentatives means tumor latency. τ is in arbitrary units.

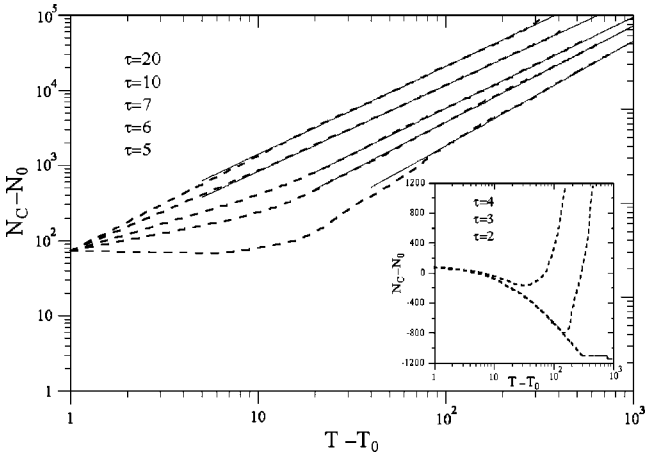

FIG. 8. Growth curves (dashed lines) for the papillary patterns under antimitotic therapy. The dose intervals used were $\tau = 20,10,7,6,5,4,3,2$ and the upper curves represent the larger intervals. For the larger dose intervals ($\tau \geqslant 5$), the tumor growth follows power laws with exponents in the range [1.2,1.4]. For shorter intervals ($\tau \leqslant 4$), the curves are shown in a semilog plot (inset). In these simulations, $\theta_{div}^{(Q)} = 0.3$ was used in addition to the parameters of Table I. Times are in arbitrary units.

branching growth [14]. Below this threshold the cell death rate equals cell division, and the tumor growth effectively stops. This qualitative behavior near the transition will probably not be observed in experimental tumors, since a very reliable determination of $\theta_{div}^{(Q)}$ is very difficult. On the other hand, experiments exhibiting both regimes, above and below the critical value, are realizable today due to the great advances made in drug delivery control. Such assays might corroborate the complex behaviors predicted by our model.

The antimitotic treatment affects both the growth and scaling laws. The compact patterns in the original model, for which the gyration radius and number of occupied sites on the tumor border scale as the square root of the total number of occupied sites (i.e., $\nu = \sigma = 1/2$), become progressively more fractal as the dose intervals are decreased. Consequently, $\nu > 1/2$ and $\sigma > 1/2$ were obtained, indicating fractal tumors with a fractal dimension given by $d_f = 1/\nu$. In general, all the tumors become more fractal when submitted to antimitotic treatments. So, there is a neat contrast with the invariance of the fractal dimension of the growing tumors under the cytotoxic treatment described in the preceding section. In Fig. 8, the increase in the number of cancer cells relative to the treatment beginning, $(N_C - N_0)$, is plotted, for distinct dose intervals, as a function of the time after the treatment beginning $(T - T_0)$. These curves suggest power laws for time evolution of the number of cancer cells with a weak dependence on the τ parameter. Indeed, we have $(N_C - N_0) \sim (T - T_0)^\beta$ with $\beta \in [1.2,1.4]$. As τ decreases, the number of tumor cells initially decays for a while, but subsequently recovers its growth (inset of Fig. 8). Below a given dose interval, N_C decreases monotonically up to a constant value.

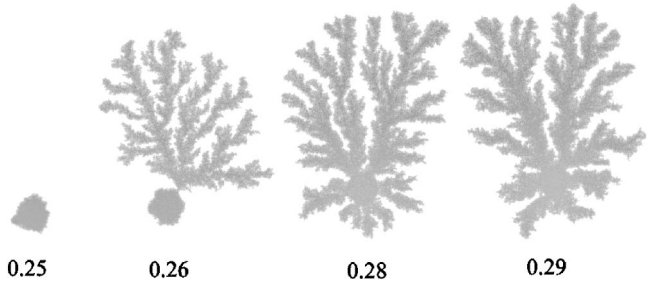

FIG. 7. Morphological transitions at $\theta_{div}^{(Q)*}$. The patterns were originally compact, and the model parameters are listed in Table I. The dose period was fixed at $\tau = 2$ and $\theta_{div}^{(Q)}$ varied around its critical value.

In order to analyze the cell division rates through the tumor, we computed the average cancer cell density ($\langle \sigma_c \rangle$) and cell division rate (w_{div}) along a longitudinal cut across the growth pattern. These average values were plotted as a function of the distance from the capillary vessel. In Fig. 9, these plots are shown for compact patterns treated with distinct τ values. For larger τ values [Fig. 9(a)] both, division rate and cancer cell density, have sharp maxima on the tumor border in front of and opposite to the capillary vessel. Notice that the peaks for division rate are significatively narrower than those for cancer cell density, demonstrating that the proliferative fraction of the tumor comprises just a small rim located at the tumor border. As the treatment is intensified (shorter τ values are considered), the cell densities through the tumors become more uniform, whereas the division rates continue exhibiting sharp maxima at the tumor borders [Figs. 9(b) and 9(c)]. If τ is sufficiently short in order to halt the tumor growth, the division rates and cancer densities become uniform along the tumor [Fig. 9(d)]. So, in these cases the division rates are counterbalanced by the death rates, leading to a vanishing net rate of cancer growth. All these results

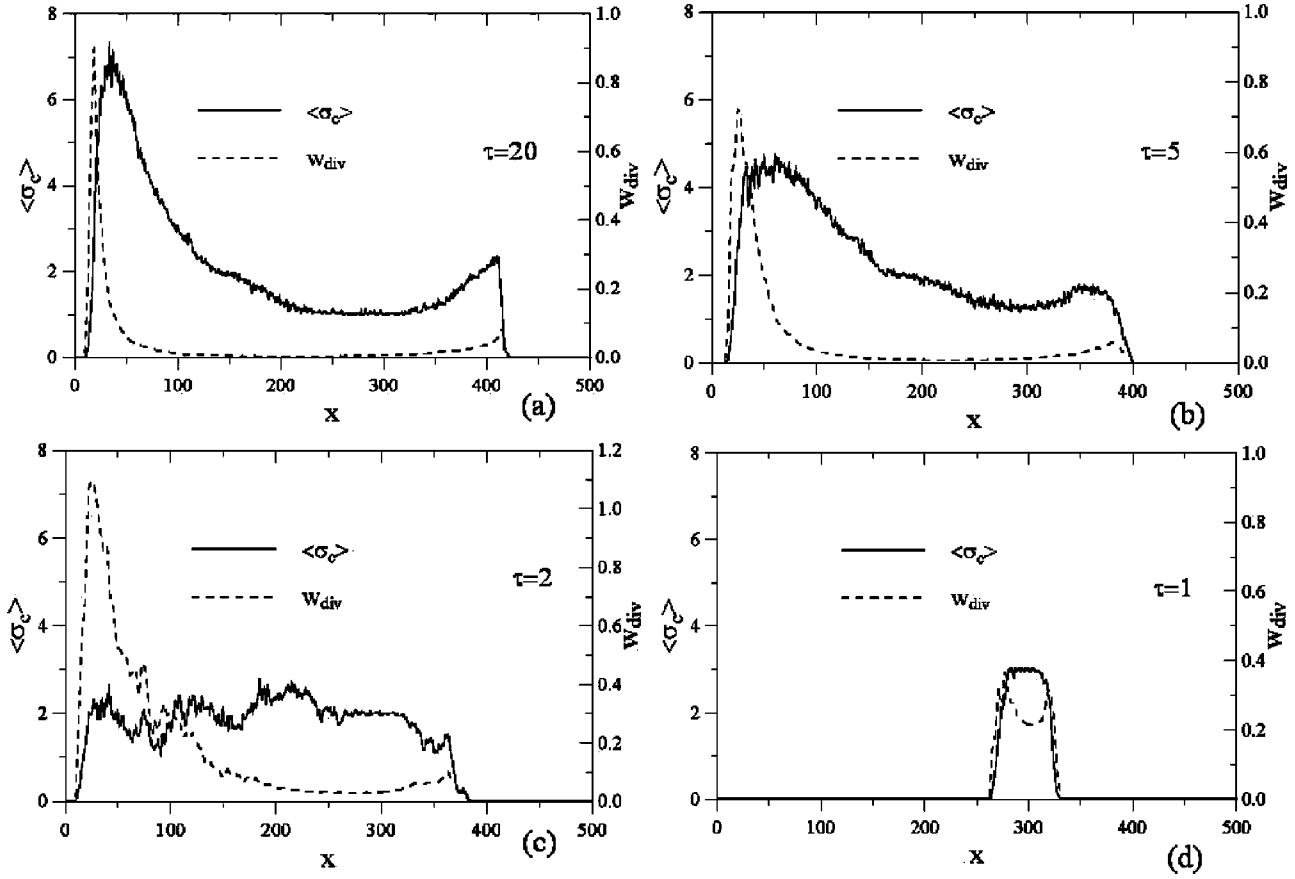

FIG. 9. Density of cancer cells σ_c (continuous lines) and division rates w_{div} (dashed lines) as a function of the distance from the capillary vessel along a longitudinal cut of the tumor. The fixed model parameters are those referent to the compact morphology indicated in Table I and $\theta_{div}^{(Q)}=0.3$. The plots correspond to (a) $\tau=20$, (b) $\tau=5$, (c) $\tau=2$, and (d) $\tau=1$. The left and right vertical axes represent σ_c and w_{div}, respectively. Distances are in lattice units.

show that the tumor patterns are altered when the mitotic properties of the cancer cells are modified by external agents.

V. CONCLUSIONS

In the present work, a reaction-diffusion model to simulate the effects of chemotherapies on the growth of carcinomas *in situ* have been studied. The model includes cell death and division, competition among cancer and normal cells by nutrients, and periodical drug administration. Two kinds of chemotherapies, using cytotoxic and antimitotic drugs, were modeled.

The main feature of this model is the use of phenomenological, macroscopic reaction-diffusion equations for nutrients and drugs controlling the stochastic actions of individual cancer cells. Such probabilistic, microscopic rules play the role of an effective kinetic model for interacting cell populations. So, from a theoretical point of view, for all cellular kinetic models, the derivation of related macroscopic equations from the microscopic description assumes great relevance. This is a difficult and not fully understood problem, which has attracted much attention [11,31] (and references therein). In particular, Lachowicz [31] mathematically discussed the diffusive and hydrodynamic macroscopic limits of a general class of kinetic models describing the evolution of individuals undergoing stochastic pairwise interactions.

In the cytotoxic model the tumors can be completely eradicated, cease their growth, or grow continuously. The last case occurs when the treatment is inefficient or the intervals between consecutive doses of drugs are large. Moreover, the morphologies and scaling laws of the growing tumor patterns are preserved. In contrast, for therapeutic approaches using antimitotic agents a morphological transition in the tumor patterns was observed. The growth patterns become progressively more fractal as more effective treatments (shorter intervals between consecutive doses and/or more efficient drugs) are considered.

Such morphological transitions are similar to recent studies claiming that bacterial colonies exposed to nonlethal concentrations of antibiotics exhibit drastic changes in their growth patterns [32]. For bacteria, these changes were imputed to variations in bacterial properties such as metabolic load and chemotaxis. In turn, normal and cancer cells cultured in monolayer and collagen gel exhibit a dynamical transition in their aggregation regimes as an adaptive response to the growth constraints imposed by high cell population density or long permanence in culture [33]. Again, the results obtained in the present work are in agreement with the point of view that cancer cells can develop an integrated defense program against stress situations similar to the re-

sponse of bacterial colonies facing severe and sustained threats [30]. However, as far as we are concerned, there are no reports on cancer literature concerning morphology transitions in the histological patterns of tumors submitted to chemotherapy. Thus, formal models similar to the one proposed in this paper, generally not familiar for most of biomedical researchers [34], can guide and refine new experiments intended to analyze such morphological transitions. Currently, experiments *in vitro* with cancer cells are being performed in our laboratories in order to investigate these morphological transitions.

It is important to mention that, usually, real effective treatments employ several therapeutic methods simultaneously [26]. So, a more realistic chemotherapeutic model should consider combined cytotoxic and antimitotic treatments. Nevertheless, in these cases relevant features such as the robustness of the tumors fractal scaling and the morphology transitions can be masked. Finally, we are modeling other cancer therapeutic strategies, such as virus and immunotoxins therapies, as well as the combination of distinct treatments, by using reaction-diffusion models similar to those considered in this paper.

ACKNOWLEDGMENTS

S. C. Ferreira, Jr. would like to thank the UFV Physics Department (Viçosa, Brazil) for the welcoming hospitality and Professor J. G. Moreira (Departamento de Física, UFMG, Brazil) for fruitful discussions. This work was partially supported by the CNPq an FAPEMIG—Brazilian agencies.

[1] D. Hanahan and R.A. Weinberg, Cell **100**, 57 (2000).
[2] J. OD McGee, P.G. Isaacson, and N.A. Wright, *Oxford Textbook of Pathology* (Oxford University Press, Oxford, 1992).
[3] R.A. Weinberg, Sci. Am. **275**(3), 62 (1996).
[4] W.H. Clark, Eur. J. Cancer **64**, 631 (1991).
[5] G.I. Evan and K.H. Vousden, Nature (London) **411**, 342 (2001).
[6] L.J. Old, Sci. Am. **275**(3), 136 (1996).
[7] J. Gómez-Navarro, D.T. Curiel, and J.T. Douglas, Eur. J. Cancer **35**, 867 (1999).
[8] J. Folkman, Sci. Am. **275**(3), 150 (1996).
[9] J.R. Bischoff *et al.*, Science **274**, 373 (1996).
[10] G.J. Pettet, C.P. Please, M.J. Tindall, and D.L.S. McElwain, Bull. Math. Biol. **63**, 231 (2001).
[11] N. Bellomo and L. Preziosi, Math. Comput. Modell. **32**, 413 (2000).
[12] H.A. Levine, S. Pamuk, B.D. Sleeman, and M. Nilsen-Hamilton, Bull. Math. Biol. **63**, 801 (2001).
[13] E. De Angelis and L. Preziosi, Math. Models Meth. Appl. Sci. **10**, 379 (2000).
[14] L.M. Sander and T.S. Deisboeck, Phys. Rev. E **66**, 051901 (2002).
[15] S.C. Ferreira, Jr., M.L. Martins, and M.J. Vilela, Physica A **261**, 569 (1998).
[16] S.C. Ferreira, Jr., M.L. Martins, and M.J. Vilela, Physica A **272**, 245 (1999).
[17] S.C. Ferreira, Jr., M.L. Martins, and M.J. Vilela, Phys. Rev. E **65**, 021907 (2002).
[18] F. Kozusco, Pao-Hsiu Chen, S.G. Grant, B.W. Day, and J. Carl Panetta, Math. Biosci. **170**, 1 (2001).
[19] F. Montalenti, G. Sena, P. Cappella, and P. Ubezio, Phys. Rev. E **57**, 5877 (1998).
[20] R.K. Sachs, L.R. Hlatky, and P. Hahnfeldt, Mathl. Comput. Modelling. **33**, 1297 (2001).
[21] J. Tervo and P. Kolmonen, Math. Models Meth. Appl. Sci. **12**, 109 (2002).
[22] J.T. Wu, H.M. Byrne, D.H. Kirn, and L.M. Wein, Bull. Math. Biol. **63**, 731 (2001).
[23] M. Scalerandi and B.C. Sansone, Phys. Rev. Lett. **89**, 218101 (2002).
[24] T.L. Jackson and H.M. Byrne, Math. Biosci. **164**, 17 (2000).
[25] M. Scalerandi, G.P. Percarmona, P.P. Delsanto, and B.C. Sansone, Phys. Rev. E **63**, 011901 (2000).
[26] S. Hellman and E.E. Volkes, Sci. Am. **275**(3), 118 (1996).
[27] J.C. Panetta, Bull. Math. Biol. **58**, 425 (1996).
[28] B.W. Feig, D.H. Berger, and G.M. Fuhrman, *The M.D. Anderson Surgical Oncology Handbook* (Lippincott Williams & Wilkins Publishers, Philadelphia, 2002).
[29] R.K. Jain, Sci. Am. **271**(1), 58 (1994).
[30] L. Israel, J. Theor. Biol. **178**, 375 (1996).
[31] M. Lachowicz, Math. Models Meth. Appl. Sci. **12**, 985 (2002).
[32] E. Ben-Jacob, I. Cohen, I. Golding, D.L. Gutnick, M. Tcherpakov, D. Helbing, and I.G. Ron, Physica A **282**, 247 (2000).
[33] R.L. Mendes, A.A. Santos, M.L. Martins, and M.J. Vilela, Physica A **298**, 471 (2001).
[34] A. Chinnaiyan *et al.*, Complexity **7**, 22 (2002).